Turbulence Measurements in Air-Water Self-Aerated Flows: Basic Analysis and Results

Hubert Chanson and Stefan Felder

The University of Queensland, School of Civil Engineering
Brisbane QLD 4072, Australia
E-mail: h.chanson@uq.edu.au

Keywords: turbulence measurements, air-water flows, signal analysis, phase-detection probes

Abstract

The two-phase gas-liquid flow properties of high-velocity open channel flows were studied experimentally in a large-size channel. The physical facility was equipped with a succession of triangular cavities associated with some strong interactions between air entrainment and flow turbulence. Detailed air-water flow measurements were collected with intrusive phase-detection probes for several flow conditions. The entire measurement technique was tested and a detailed sensitivity analysis was performed to assess the optimum sampling rate and duration. The new two-phase flow measurements demonstrated the high levels of turbulence in the high-speed, highly turbulent free-surface flows. These were highlighted by a strong rate of kinetic energy dissipation and dimensionless shear stress.

Introduction

In high-speed open channel flows, the interaction between the highly turbulent waters and the atmosphere is associated with some major deformation, twist and warp of the free-surface. Across the air-water interface, some air is continuously entrapped while water droplets are ejected. The resulting air-water flow mixture extends through the entire air-water column as illustrated by photographs and laboratory observations (Kobus 1984, Wood 1991, Chanson 1997) (Fig. 1). The white waters are a complex two-phase gas-liquid flow motion with the void fractions ranging from small, often non-zero values close to the invert to 100% above the free-surface. The latter is usually defined as the location where the void fraction equals 90% because the air-water flow behaves as a homogenous mixture below while ejected droplets and splashing tend to have a free-fall trajectory for void fractions larger than 95% (Cain and Wood 1981, Chanson 1997, Chanson and Carosi 2007). A basic feature of the white waters is the level of interactions between the air-water structures and the turbulence (Brocchini and Peregrine 2002, Chanson and Toombes 2002, Chanson and Carosi 2007). Recent experimental findings hinted that the intermediate region where the void fraction ranges from 30% to 70% may play a major role in terms of turbulent energy dissipation (Chanson and Carosi 2007, Felder and Chanson 2009).

To date, relatively limited data are available on the two-phase gas-liquid properties of these high-speed free-surface flows despite five decades of experimental measurements. A knowledge gap encompasses the turbulence characteristics in the two-phase gas-liquid flow region. The experimental methods rely primarily on the use of intrusive phase-detection probes based upon the needle probe design introduced in the 1960s (Neal and Bankoff 1963). The needle probe design is considered as the most reliable intrusive phase detection probe design (Jones and Delhaye 1973, Bachalo 1994, Chanson 1997). This type of sensor is designed to pierce bubbles and droplets. The sensor itself may be an optical fibre or conductivity/resistivity probe. The principle behind the optical probe is the change in optical index between the two phases (Cartellier 1992, Cartellier and Barrau 1998). The conductivity probe is based upon the difference in electrical resistivity between air and water. (Herringe 1973, Serizawa et al. 1975). While the most recent measurement techniques are based upon the same sensor design, some recent advances in signal processing led to some advancement and new turbulence characteristic measurements (Chanson 2002, Chanson and Carosi 2007b).

In the present study, the two-phase gas-liquid flow properties of high-speed open channel flows were studied experimentally in a large-size channel with triangular cavities (Fig. 2). The physical facility was selected for the level of strong interactions between air entrainment and flow turbulence. Detailed turbulence data were collected with intrusive phase-detection probes for several discharges. First the entire measurement technique was tested and a detailed sensitivity analysis was performed to assess the effects of sampling rate and duration on the multiphase flow properties. Using the validated metrology, data acquisition and signal processing, some new two-phase flow measurements were performed in the high-speed, highly turbulent free-surface flows.

(A) General view of the dam spillway operation seen from the left bank (shutter speed: 1/800 s)

(B) Details of the free-surface and white waters (shutter speed: 1/1,000 s)

Figure 1: Free-surface aeration down the North Pine spillway on 22 May 2009. Dam height: 40m, dam completion: 1976.

Nomenclature

C	void fraction defined as the volume of air per unit volume of air and water
C_{mean}	depth-averaged void fraction: $C_{mean} = 1/Y_{90} \int_0^{Y_{90}} C\, dy$
c	instantaneous void fraction: c = 0 in water and c = 1 in air
D_H	hydraulic diameter (m) or equivalent pipe diameter
d	equivalent clear water flow depth (m): d = $(1-C_{mean})Y_{90}$
d_c	critical flow depth (m): $d_c = \sqrt[3]{Q_w^2/(g\,W^2)}$
E	specific energy (m)
F	bubble count rate (Hz) defined as half the number of air-water interfaces impacting the probe sensor per unit time
F_{max}	maximum bubble count rate (Hz) in a cross-section
f	Darcy-Weisbach friction factor
g	gravitational constant (ms^{-1})
H	total head (m)
H_{max}	upstream total head (m) above the sampling location
h	vertical step height (m)
K	inverse of the dimensionless expansion rate of the shear layer
L_I	distance (m) from the channel upstream end to the onset of free-surface aeration
l	horizontal step length (m)
Q_w	water discharge (m^3s^{-1})
q_w	water discharge per unit width (m^2s^{-1})
Re	Reynolds number defined as: $Re = \rho_w U_w D_H / \mu_w$
Tu	turbulence intensity
U_w	depth-averaged flow velocity (ms^{-1})
V	air-water interfacial velocity (ms^{-1})
V_{90}	characteristic velocity (ms^{-1}) at $y = Y_{90}$
W	channel width (m)
x	longitudinal distance (m)
Y_{90}	characteristic distance (m) where C = 90%
y	distance (m) normal to the pseudo-bottom formed by the step edges

Greek letters

θ	angle between the pseudo-bottom formed by the step edges and the horizontal
ρ_w	water density (kgm^{-3})
μ_w	water dynamic viscosity (Pas)

Subscripts

air	air
max	maximum value in a cross-section
w	water
90	flow conditions were $y = Y_{90}$

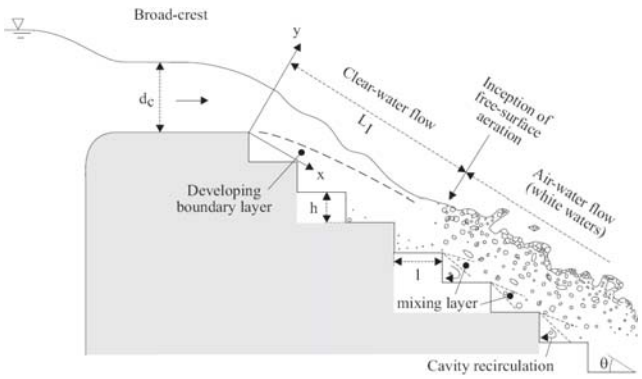

(A) General view of the experiment

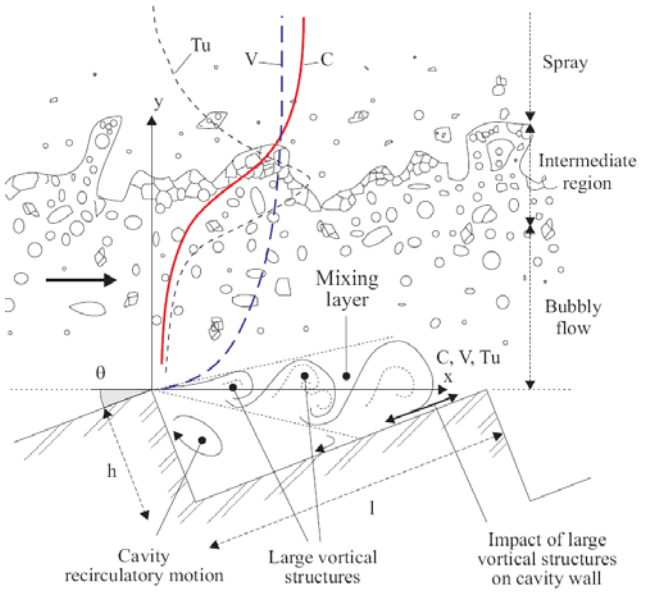

(B) Details of the cavity flow

Figure 2: Free-surface aeration in a skimming flow above a stepped spillway

Experimental Facility and Instrumentation

New experiments were conducted at the University of Queensland in a 3.2 m long, 1 m wide chute with flow rates ranging from 0.014 to 0.250 m^3s^{-1}. The chute consists of a broad-crest followed by 10 identical steps (h = 0.10, l = 0.20 m, 26.6º slope). The open channel facility is a permanent facility and the inflow quality has been verified in this and previous studies (Jempson 2001, Gonzalez and Chanson 2007). Waters are supplied by a pump controlled with adjustable frequency AC motor drive enabling an accurate discharge adjustment. The water discharge was measured from the upstream head above the crest, and the head-discharge relationship was checked with detailed velocity distribution measurements on the crest itself (Gonzalez and Chanson 2007). The air-water flow properties were measured using an array of two single-tip resistivity probes (⌀ = 0.35 mm, Pt) and a double-tip resistivity probe (⌀ = 0.25 mm, Pt). In the latter, the longitudinal separation between tips was 7.5 mm. Both phase detection probes were excited by an electronic system (Ref. UQ82.518) designed with a response time less than 10 μs and calibrated with a square wave generator. The probe signals were sampled at 20 kHz per sensor for 45 s (see below).

The translation of the probes in the direction normal to the pseudo-bottom formed by the step edges was controlled by a fine adjustment traverse mechanism connected to a Mitutoyo™ digimatic scale unit with an accuracy of less than 0.2 mm.

Experimental flow conditions

On a stepped chute, the waters flow as a succession of free-falling nappes at low flow rates. At each step edge, the flow takes off and hits the step below as a free-falling jet, sometimes followed by a hydraulic jump. The energy dissipation occurs by jet breakup in air, by jet impact the following step, and with the formation of a fully developed or partial hydraulic jump. At large flow rates with an identical chute geometry (step height, mean slope), the water skims over the pseudo-invert formed by the step edges (i.e. skimming flow) as a coherent stream cushioned by the recirculating fluid trapped between them (Fig. 2 & 3). The external edges of the steps form a pseudo-bottom over which the waters flow. In the triangular cavities, some recirculating vortices develop and are maintained through the transmission of shear stress from the water flowing past the edge of the steps. At the upstream end, the flow is non-aerated. After a few steps the flow is characterised by a strong air entrainment and by vortices at the step toes (Fig. 2 & 3). For some intermediate discharges, a transition flow regime is observed, characterised by a chaotic behaviour and strong splashing and droplet projections downstream of the inception point of free-surface aeration. The transition flow exhibits some significant longitudinal variations in flow properties between adjacent steps. The flow seems very chaotic and does not present the coherent appearance of skimming flows.

The present observations indicated a nappe flow regime for dimensionless discharges $d_c/h < 0.5$ and a skimming flow regime for $d_c/h > 0.9$, where d_c is the critical flow depth: $d_c = \sqrt[3]{Q_w^2/(g\,W^2)}$ and h is the vertical step height. The results were in agreement with the literature (Chanson 2001).

The air-water flow measurements were conducted with dimensionless discharges d_c/h between 1.01 and 1.85. The probe sensors were located on the channel centreline at the step edges for all flow rates. The flow conditions corresponded to Reynolds numbers ranging from 4×10^5 to 1.0×10^6 where $Re = \rho_w U_w D_H/\mu_w$ with ρ_w and μ_w the water density and viscosity respectively, U_w the flow velocity and D_H the hydraulic diameter (or equivalent pipe diameter). The details are summarised in Table 1 and compared with earlier studies conducted on slopes of 1:2.5 and 1:3.5 with large Reynolds numbers to minimise the potential scale effects. These were specifically discussed by Chanson (2009) and Felder and Chanson (2009).

(A) $d_c/h = 1.15$, $Re = 4.85\times10^5$, inception of free-surface aeration at step edge 4

(B) d_c/h = 1.85, Re = 9.9×10^5, inception of free-surface aeration at step edge 8

Figure 3: Photographs of skimming flows (present study).

Ref.	θ °	h m	d_c/h	Re	Sampling
Chanson & Toombes (2002)	15.9 21.8	0.10	0.63 to 1.9 0.54 to 1.49	2×10^5 to 1×10^6 1.6×10^5 to 7×10^5	20 kHz for 20 s per sensor (∅=0.025 mm)
Gonzalez & Chanson (2004)	15.9	0.05 0.10	0.7 to 3.2 0.83 to 1.70	8×10^4 to 8×10^5 3×10^5 to 8.7×10^5	20 kHz for 20 s per sensor (∅=0.025 mm)
Chanson & Carosi (2007)	21.8	0.10	1.0 to 1.57	3.8×10^5 to 7.1×10^5	20 kHz for 45 s per sensor (∅=0. 25 mm)
Felder & Chanson (2009)	21.8	0.05	1.17 to 3.05	1.7×10^5 to 6.9 10^5	20 kHz for 45 s per sensor (∅=0.25 mm)
Present study	26.6	0.10	1.0 to 1.85	4×10^5 to 1×10^6	20 kHz for 45 s per sensor (∅=0.25 mm)

Table 1: Experimental investigations of air-water flow properties down stepped chutes.

Signal Processing and Data Analysis

The measurement principle of phase-detection intrusive probes is based upon the difference in optical index or electrical resistivity between air and water. The intrusive probe sensor is designed to pierce the incoming bubbles, droplets and gas-liquid interfaces. A typical signal output is shown in Figure 4. The signal processing may be conducted on the raw signal output and on a thresholded "square wave" signal (Fig. 4). The thresholded signal analysis relies upon some arbitrary discrimination between the two phases. The technique may be based upon single or multiple thresholds, or some signal pattern recognition. The resulting square-wave signal yields the instantaneous void fraction c: c = 0 in water and c = 1 in air (Fig. 4B). It is used to calculate the time-averaged void fraction, bubble count rate, the air/water chord times, the bubble/droplet chord lengths and their statistical moments (mean, median, std, skewness, kurtosis), and the streamwise particle grouping analysis.

In high-velocity free-surface flows, the most robust discrimination technique is the single threshold technique with a threshold set at about 45-55% of the air–water voltage range (Toombes 2002, Chanson and Carosi 2007b). Figure 4B illustrates the single-threshold output using a 50% threshold.

A series of sensitivity analysis experiments were conducted in the stepped chute to assess the effect of a number of parameters on the two-phase flow properties. The flow conditions are summarised in Table 2. A typical example is presented in Figure 5, showing the effect of the single threshold level on the time-averaged void fraction C and bubble count rate F. The results suggest that a threshold level between 25% and 85% has little effect on the void fractions data as found by Herringe and Davies (1974), but the bubble count rate data were more sensitive to the threshold level (Fig. 5). Herein the experimental data were processed with a single threshold set at 50% of the air-water range that was deemed to be an optimum to investigate the air-water column in the high-velocity free-surface flows.

Ref.	Q m^3s^{-1}	d_c/h	Re	Flow regime	Sampling
TRA	0.058	0.70	2.3×10^5	Transition	Step edge 10
SK	0.173	1.45	6.9×10^5	Skimming	Step edge 10

Table 2: Sensitivity analysis tests.

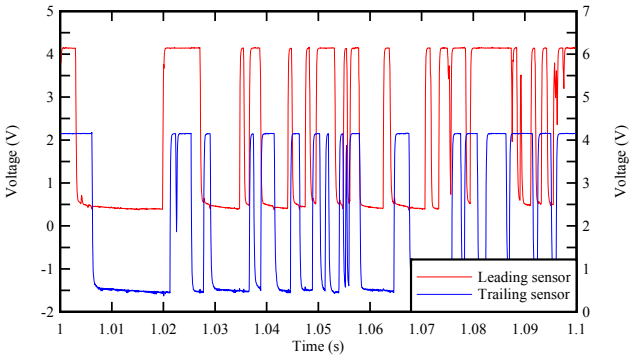

(A) Raw probe output

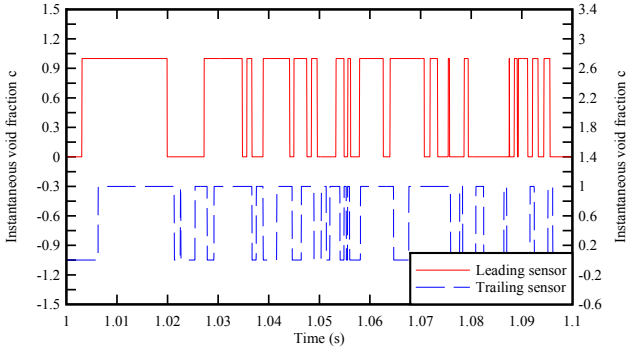

(B) Thresholded signal (single-treshold (50%))

Figure 4: Probe signal output: d_c/h = 1.29, Re = 5.6×10^5, step edge 9, C = 0.59, F = 161 Hz, V = 3.75 m/s.

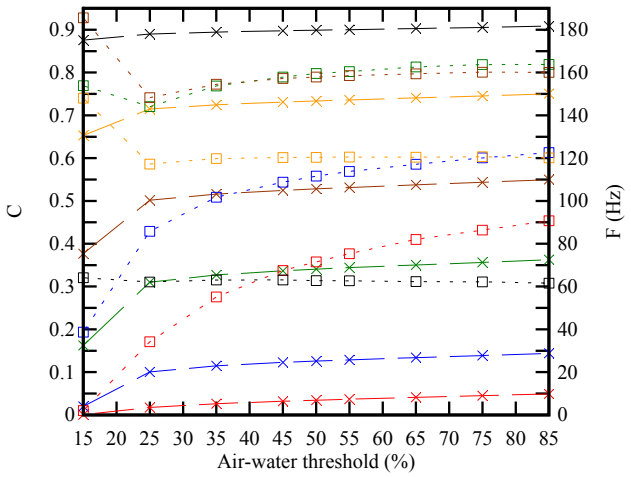

Figure 5: Effect of the air-water threshold on the time-averaged void fraction C (× symbols) and bubble count rate F (square symbols) in a high-velocity open channel flow. Sampling rate: 20 kHz per sensor, sampling duration: 45 s, sensor size: 0.25 mm.

Basic air-water flow properties

The time-averaged void fraction C is the proportion of time that the probe sensor spends in the air. Past experiences suggested that the sensor orientation has little effect on the void fraction data, but it must be stressed that the phase-detection probe sensors are designed to pierce the bubbles/droplets with minimum interference. Simply the probe sensor should face the bubbles/droplets as illustrated in Figure 6. The bubble count rate F is defined as the number of bubbles impacting the probe tip per second in a bubbly flow. More generally, it is calculated as half the number of gas-liquid interfaces detected by the probes. It is noteworthy that the bubble count rate and void fraction are related. In a free-surface flow, the experimental data showed some form of parabolic relationship:

$$[1] \qquad \frac{F}{F_{max}} = 4\,C\,(1-C)$$

where F_{max} is the maximum bubble frequency in the cross-section. Toombes and Chanson (2008) demonstrated the theoretical validity and advanced a more general expression.

When two or more phase detection sensors are simultaneously sampled, a correlation analysis provides some additional information on the bubbly flow properties. A well-known application is the use of dual tip probe in which the two sensors are aligned with the flow direction (Fig. 6). For a range of void fractions ($0.02 < C < 0.98$), a cross-correlation analysis between the two probe sensor outputs gives the time averaged interfacial velocity V. The turbulence intensity Tu may be derived from the relative width of the cross-correlation function (Chanson and Toombes 2002). More generally, when two probe sensors are separated by a transverse or longitudinal distance, their signals may be analysed in terms of the auto- and cross-correlation functions (Chanson and Carosi 2007).

Herein a detailed sensitivity analysis was conducted to assess the impact of the air-water threshold, sampling rate and duration on the basic air-water flow properties over the entire air-water column (Table 2). Some basic results are regrouped in Figures 5, 7 and 8. The results demonstrated that the sampling frequency had to be greater than 10 kHz, with little differences between the sampling rates of 20 and 40 kHz per sensor. The sampling duration had to be greater than 20 s to have negligible effects on the void fraction, bubble count rate and air-water velocity, while the advanced correlation analyses including the estimate of the turbulence intensity required a sampling duration of 45 s or larger. Overall the findings justified the selection of the sampling rate and duration (20 kHz, 45 s) used during the present study.

Figure 6: Photograph of the dual-tip conductivity probe (Ø = 0.25 mm). Top: Three-quarter view, flow from bottom left to top right, Re = 3.5×10^5. Bottom: Looking downstream at the probe tip, $d_c/h = 1.59$, Re = 7.9×10^5.

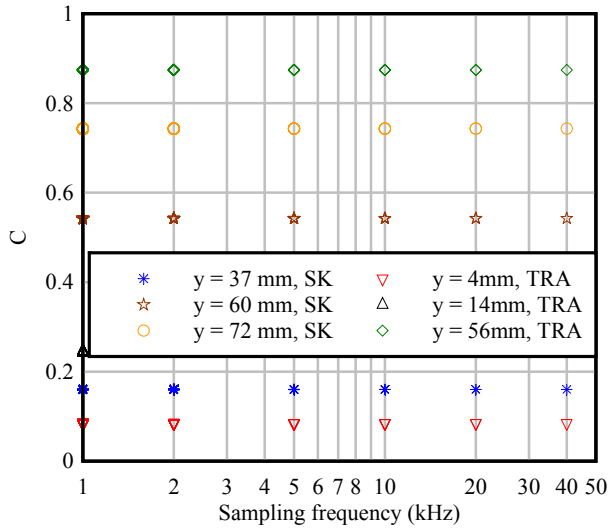

(A) Effect on the void fraction C

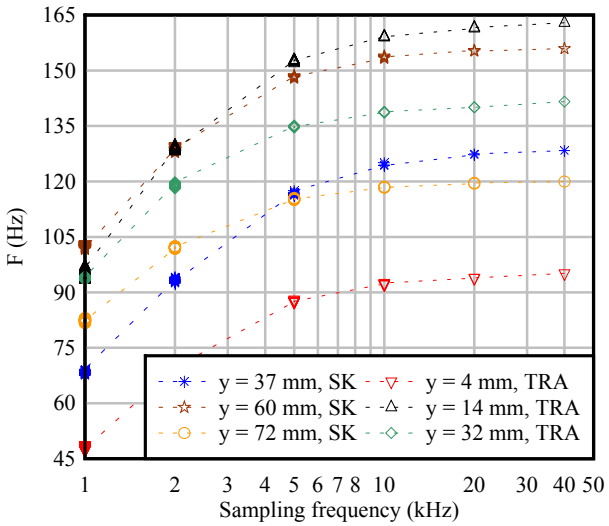

(B) Effect on the bubble count rate F

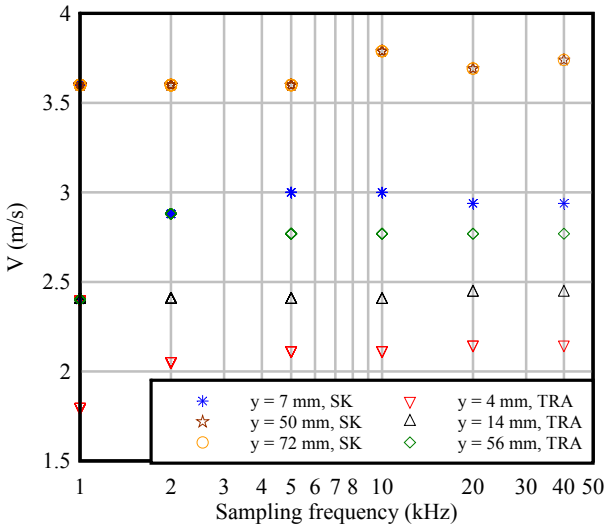

(C) Effect on the air-water interfacial velocity V

Figure 7: Effect of the sampling frequency on the void fraction, bubble count rate and interfacial velocity measurements in a high-velocity open channel flow. Air-water threshold: 50%, sampling duration: 45 s, sensor size: 0.25 mm.

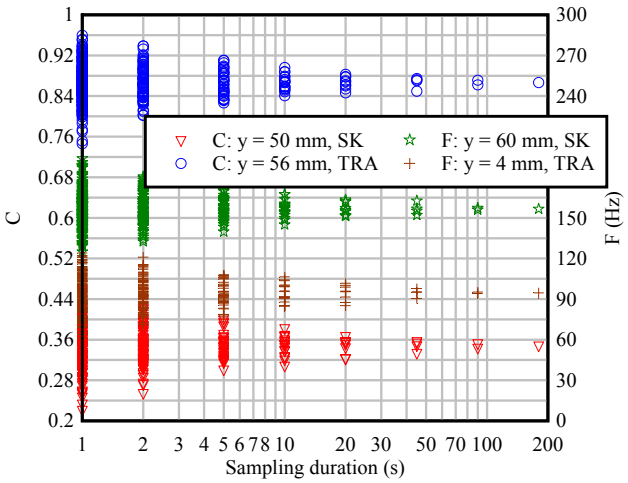

(A) Effect on the void fraction C and bubble count rate F

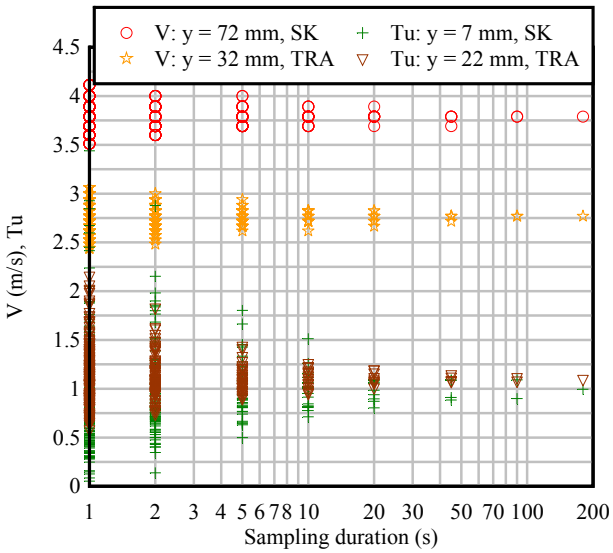

(B) Effect on the air-water interfacial velocity V and turbulence intensity Tu

Figure 8: Effect of the sampling duration on the void fraction, bubble count rate, interfacial velocity and turbulence intensity measurements in a high-velocity open channel flow. Air-water threshold: 50%, sampling frequency: 20 kHz, sensor size: 0.25 mm.

Basic Results

On the steep stepped chute, the open channel flow non-aerated at the upstream end of the chute (Fig. 2A & 3). The air entrainment occurred when the turbulent shear next to the free-surface exceeded the resistance offered by surface tension and buoyancy. Downstream, some intense air-water mixing took place and large amounts of air were entrained. The observations indicated some very-strong interactions between main stream turbulence, step cavity recirculation zones and free-surface which were associated with some turbulent dissipative processes.

The location L_I of the inception point of free-surface aeration was observed. L_I represents the longitudinal distance measured from the downstream end of the broad-crest (Fig. 2A). The results are presented in a dimensionless form in Figure 9 in which the observations are compared with the empirical correlation:

(2)

$$\frac{L_I}{h\cos\theta} = 9.719\,(\sin\theta)^{0.0796}\left(\frac{q_w}{\sqrt{g\sin\theta\,(h\cos\theta)^3}}\right)^{0.713}$$

where θ is the angle between the slope formed by the step edges and the horizontal, q_w is the water discharge per unit width ($q_w = Q_w/W$) and g is the gravity acceleration. Equation (2) was developed for and validated with prototype and laboratory steep stepped chute data (Chanson 1994,2001). It is shown in Figure 4 for $\theta = 26.6°$ and compared with present and earlier experimental data sets. All data highlighted that the location of the air entrainment inception L_I moved downstream with increasing flow rate.

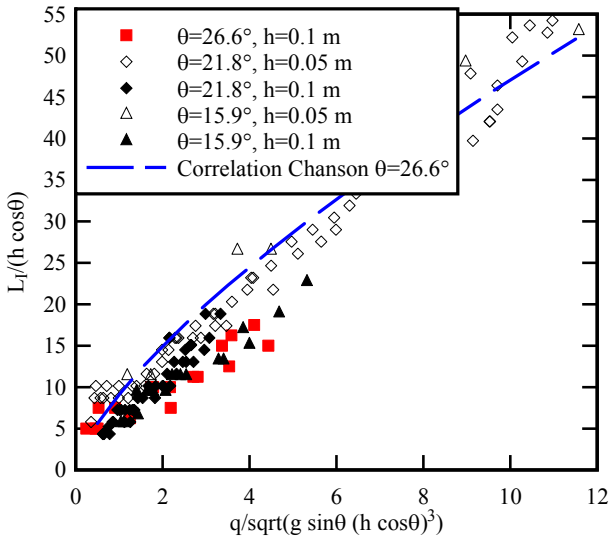

Figure 9: Dimensionless location $L_I/(h\cos\theta)$ of the inception point of free-surface aeration on stepped spillways - Comparison with Equation (2) calculated for θ = 26.6º

Air-water flow properties

Downstream of the inception point of free-surface aeration, both visual observations and intrusive measurements showed some substantial free-surface aeration, and the flow aeration remained sustained downstream all along the chute (Fig. 2 & 3). Figure 10 illustrates some typical dimensionless distributions of void fraction, bubble count rate and velocity downstream of the inception point.

In the skimming flow, the void fraction distributions followed a smooth S-shape that was modelled by an analytical solution of the advective diffusion for air bubbles:

$$C = 1 - \tanh^2\left(K' - \frac{y'}{2\times D_o} + \frac{\left(y' - \frac{1}{3}\right)^3}{3\,D_o}\right) \quad (3)$$

where $y' = y/Y_{90}$, y is the distance measured normal to the pseudo-invert formed by the step edges, Y_{90} is the characteristic distance where C = 90%. K' is an integration constant and D_o is a function of the depth-averaged void fraction C_{mean} only. Equation (3) was first developed by Chanson and Toombes (2002) and it is compared with experimental data in Figure 10.

The dimensionless distributions of bubble count rate showed consistently a characteristic shape with a maximum value F_{max} observed for void fractions between 0.40 and 0.55. This is seen in Figure 10 with the dimensionless count rate data F/F_{max}. A characteristic feature of all the experiments (not shown in Fig. 10) was a distinct seesaw pattern in terms of the dimensionless maximum bubble count rate $F_{max}d_c/V_c$ and depth-averaged void fraction C_{mean}. The longitudinal oscillations had a wave length of about two step cavities. This pattern was observed for a range of slopes and step heights (Boes 2000, Chanson and Toombes 2002, Yasuda and Chanson 2003, Felder and Chanson 2009) and it is thought to be caused by the strong interferences between the vortex shedding in the shear layers behind each step edge and the free-surface (Fig. 2B & 3).

The dimensionless distributions of interfacial velocity showed a self-similar shape. At each step edge, the velocity distributions compared favourably with a power-law function for $y' = y/Y_{90} < 1$ and with an uniform profile for $y/Y_{90} > 1$:

$$\frac{V}{V_{90}} = y'^{1/N} \quad (4)$$

$$\frac{V}{V_{90}} = 1 \quad (5)$$

where V_{90} is the characteristic air-water velocity at $y = Y_{90}$. Equations (6) and (7) are compared with the data in Figure 10. Herein, the velocity power law exponent 1/N was about 1/10 in average (i.e. N = 10), but it varied between adjacent step edges. For example, in Figure 10, the velocity data were close to a 1/7th power law. The fluctuations in velocity power law exponent were believed to result from the complicated interference between adjacent shear layers and cavity flows.

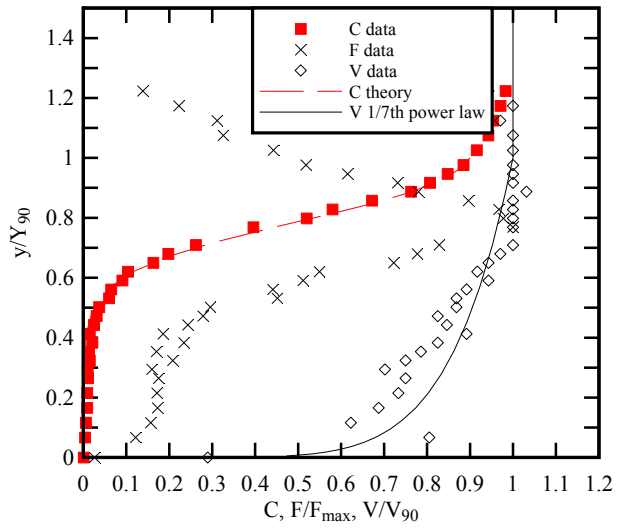

Figure 10: Dimensionless distributions of void fraction C, bubble count rate F/F_{max} and velocity V/V_{90} in air-water skimming flows on a stepped spillway: d_c/h = 1.85, Re = 1×10^6, step edge 10, Y_{90} = 0.101 m, V_{90} = 4.54 m/s, F_{max} = 76.4 Hz, C_{mean} = 0.21.

Typical distributions of turbulent intensity are presented in Figure 11. The turbulent intensity profiles exhibited some maximum turbulence level for $0.3 \le y/Y_{90} \le 0.7$ (Fig. 11A). The experimental data showed further a strong correlation between the turbulence intensity Tu and the dimensionless bubble count rate Fd_c/V_c. This is illustrated in Figure 11B which presents the turbulence intensity Tu as a function of the bubble count rate. The data collapsed reasonably well into a linear trend:

$$Tu = 0.35 + 0.032\left(\frac{F\,d_c}{V_c}\right) \quad (6)$$

While the quantitative result differs from earlier studies (Chanson and Carosi 2007), Equation (6) demonstrated a monotonic increase in turbulence levels with an increase in bubble count rate. The limit for zero bubble count rate (i.e. Tu = 0.35) was close to monophase flow measurements on a stepped chute and above d-type roughness (Amador et al. 2006, Tachie and Adane 2007). It is proposed that the continuous twist and warp of the air-water interfacial structure induced some large turbulence levels that were measured by the double-tip conductivity probe.

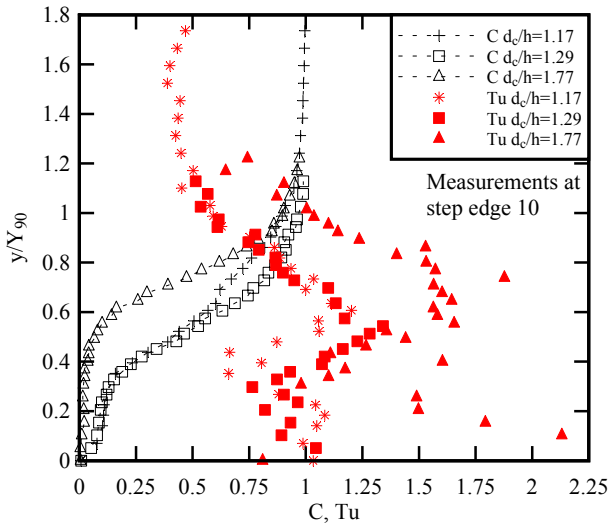

(A) Normal distributions of turbulence intensity and void fraction: d_c/h = 1.17, 1.29 & 1.77

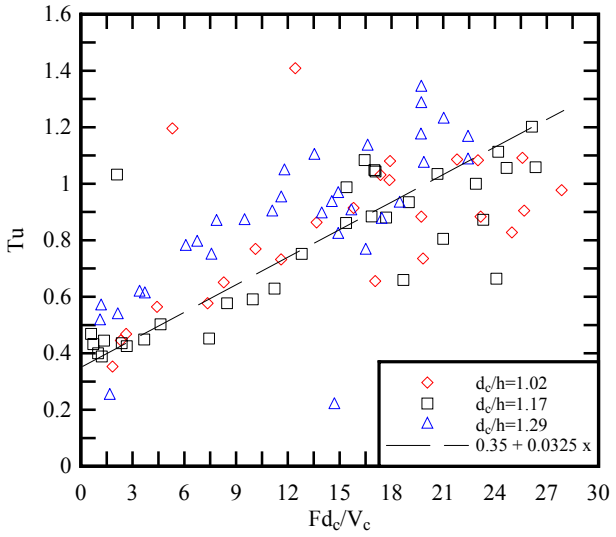

(B) Turbulence intensity versus bubble count rate: d_c/h = 1.02, 1.17 & 1.29 - Comparison with Equation (6)

Figure 11: Dimensionless distributions of turbulence intensity and void fraction in air-water skimming flows on a stepped spillway: All measurements at step edge 10.

However the data scatter must be noted (Fig. 2). This was typical to all data sets and it appeared to be related to some variations in the auto-correlation function properties within a cross-section.

Turbulent kinetic energy dissipation and boundary friction

The rate of energy dissipation $\Delta H/H_{max}$ was estimated at several steps along the chute based upon the detailed air-water flow measurements. H_{max} is the upstream total head above the step location, $\Delta H = H_{max} - E$, and E is the specific energy of the flow at the sampling location:

$$E = d\cos\theta + \frac{U_w^2}{2g} \quad (7)$$

where d is the equivalent clear water depth ($d = (1-C_{mean})Y_{90}$) and U_w is the flow velocity ($U_w = q_w/d$). The total head H is proportional to the total energy per unit volume and the specific energy E equals the total head using the local bed elevation as potential energy reference (Henderson 1966). The present results showed systematically a decreasing rate of energy dissipation on the stepped chute with increasing discharge from about $\Delta H/H_{max}$ = 60% for $d_c/h < 1.2$ down to 50% for d_c/h = 1.85. The trend was consistent with earlier studies (Matos 2000, Chanson 1994,2001). The present results were obtained with a fully-developed, aerated flow at the stepped chute downstream end. For larger discharges, the flow might not be fully-developed before the downstream end, and the rate of turbulent energy dissipation could be considerably smaller.

The high-velocity skimming flow was characterised by some significant form losses (Fig. 2). Some dissipation mechanisms are sketched in Figure 2B. Downstream of the inception point of air entrainment, the average turbulent shear stress between the high-speed flows and the recirculation motion was deduced from the measured slope of the total energy line. The dimensionless boundary shear stress may be expressed in terms of a dimensionless friction coefficient:

$$f = \frac{8\,g\left(-\frac{\partial H}{\partial x}\right)\left(\int_{y=0}^{Y_{90}}(1-C)\,dy\right)}{U_w^2} \quad (8)$$

where f is the equivalent Darcy-Weisbach friction factor of the air-water skimming flow, and the term $(-\partial H/\partial x)$ is the slope of the total head line (Henderson 1966). The data are presented in Figure 12 where the friction factor is shown as a function of the dimensionless cavity height $h\cos\theta/D_H$, where D_H is the hydraulic diameter. $h\cos\theta$ represents the cavity depth measured normal to the flow direction.

In average, the equivalent Darcy friction factor was $f \approx 0.22$ downstream of the inception point of air entrainment for the present study. The findings indicated larger turbulent shear stresses than on a smooth chute and these were consistent with experimental study of open channel flows past d-type roughness (Coleman et al. 1997, Tachie and Adane 2007). The present results are compared with earlier data sets (Table 1) in Figure 12. All the laboratory data were close and compared favourably with a simplified analytical model of the maximum shear stress in the developing shear layer downstream of each step edge. The latter may be expressed in dimensionless form as: $f = 2/(K\sqrt{\pi})$ where 1/K is the dimensionless expansion rate of the shear layer (Chanson et al. 2002). The theoretical expression predicts f = 0.2 for K = 6 that is close to the observations (Fig. 12).

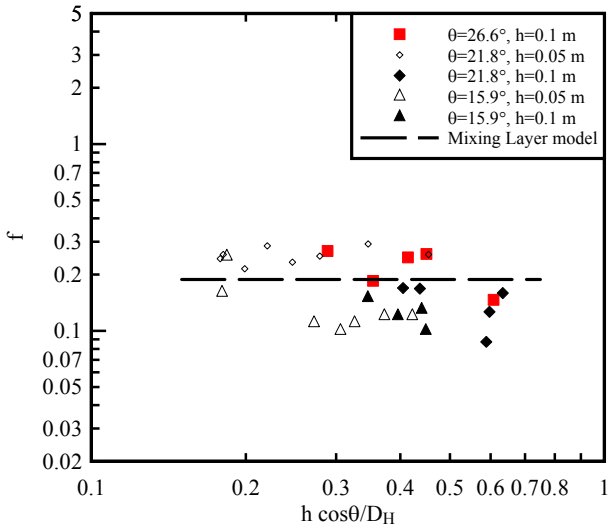

Figure 12: Friction factor f for high-velocity air-water flows on a stepped channel.

Discussion

In a high-speed skimming flow above the stepped, triangular cavities, the basic mechanisms of turbulent dissipation included cavity recirculation, momentum exchange with the free stream, and interactions between free-surface and mainstream turbulence. The interactions between mixing layer and horizontal step face, and skin friction at the step downstream end contributed to further energy dissipation on moderate slopes (Lin and Rockwell 2001). At each step edge, highly coherent small-scale vortices were formed abruptly at the step corner because of the large gradient of vorticity at the corner. The initial region of the mixing layer was dominated by a train of sequential small-scale vortices which paired to form large scale vortical structures that were advected downstream. The three dimensional nature of recirculating vortices is believed to play a role to further the rate of energy dissipation. Gonzalez and Chanson (2008) demonstrated quantitatively some means to enhance the flow resistance with passive turbulence manipulation of the cavity recirculation motion. More recently Carosi and Chanson (2008) showed some turbulent energy dissipation in the bulk of the aerated flow in the form of large-scale vortices. The turbulent structures were produced in the developing shear layers and cavity region, ejected into the main flow and interacted with the "free-surface". The dissipation process was linked with both the entrapment and advection of air bubbles within the main flow and the formation and ejection of water droplets above the "free-surface".

Further features of the cavity recirculation motion included the simultaneous occurrence of outflows of fluid from the cavities as well as inflows into the cavities, together with a sequential cavity ejection process. Visual observations showed a pattern similar to the sequential ejection phenomenon observed in boundary layer flow past d-type roughness (Djenidi et al. 1999). Figure 13 presents a sketch of two successive cavity ejection. It is believed that the initiating mechanism for the cavity outflows is likely to be triggered by the skimming flow rather than by the cavity recirculatory motion (Djenidi et al. 1998, Gonzalez and Chanson 2008).

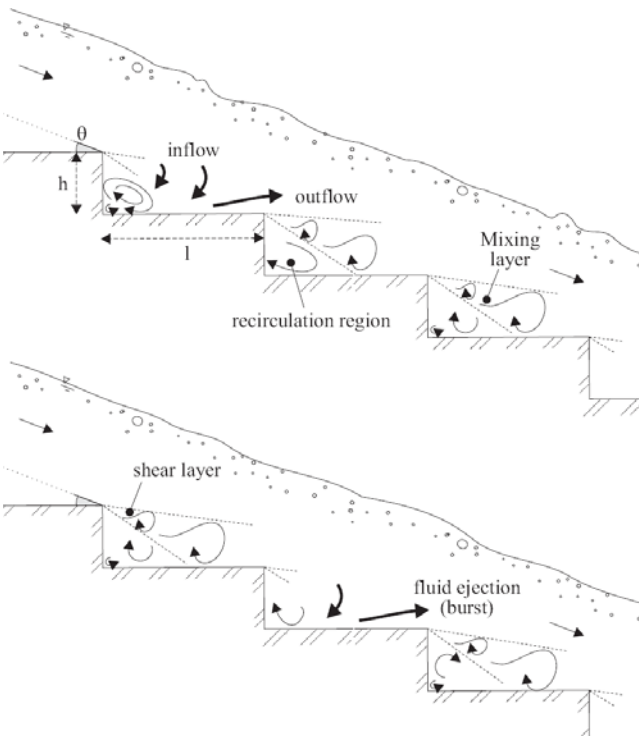

Figure 13: Sequential cavity ejection process in a high-velocity skimming flow above a stepped chute. Sketch representing the cavity ejections of two adjacent cavities.

Conclusions

The present study focused on high-velocity open channel flows and the deformation, twist and warp of the free-surface that are associated with major free-surface aeration. The two-phase gas-liquid flow properties were studied experimentally in a large-size channel with triangular cavities. Some detailed measurements were collected in the air-water flow with intrusive phase-detection probes. The entire measurement technique was tested and a detailed sensitivity analysis was performed to assess an optimum sampling rate and duration. The optimum sampling rate and duration were found to be 20 kHz and 45 s using a single-threshold technique set at 50% of the air-water range. The experiments demonstrated that, for the investigated flow conditions, the sampling rate had to be greater than 10 kHz, with a sampling duration equal to or larger than 45 s.

In the air-water skimming flows, the new two-phase flow measurements demonstrated the high levels of turbulence in the high-speed, highly turbulent free-surface flows. These were highlighted by a strong rate of kinetic energy dissipation and large dimensionless shear stresses. The equivalent Darcy friction factor was $f \approx 0.22$ in average downstream of the inception point of air entrainment. The data compared favourably with a simplified analytical model of the maximum shear stress in the developing shear layer downstream of each step edge.

Lastly it must be stressed that most detailed gas-liquid flow measurements were performed in laboratory under controlled flow conditions. A challenge remains to conduct field measurements in a prototype facility (e.g. Fig. 1)

operating with Reynolds numbers typically between 10^7 and 10^9.

Acknowledgements

The authors acknowledge the technical assistance of Ahmed Ibrahim, Graham Illidge and Clive Booth. Some experimental measurements were undertaken by Rhys Collins and Henry Cheung.

References

Amador, A., Sanchez-Juny, M., and Dolz, J. Characterization of the Nonaerated Flow Region in a Stepped Spillway by PIV. Jl of Fluids Eng., ASME, Vol. 128, No. 6, pp. 1266-1273 (2006)

Bachalo, W.D. Experimental methods in Multiphase Flows. Intl Jl of Multiphase Flow, Vol. 20, Suppl., pp. 261-295 (1994)

Boes, R.M. Zweiphasenstroömung und Energieumsetzung an Grosskaskaden. ('Two-Phase Flow and Energy Dissipation on Cascades.') Ph.D. thesis, VAW-ETH, Zürich, Switzerland (in German). (also Mitteilungen der Versuchsanstalt fur Wasserbau, Hydrologie und Glaziologie, ETH-Zurich, Switzerland, No. 166) (2000)

Brocchini, M., and Peregrine, D.H. Interaction of Strong Turbulence with Free Surfaces. World Scientific, Advances in Coastal and Ocean Engineering Series, Vol. 8, Singapore (2002)

Cain, P., and Wood, I.R. Measurements of Self-aerated Flow on a Spillway. Jl Hydraulic Div., ASCE, 107, HY11, pp. 1425-1444 (1981)

Carosi, G., and Chanson, H. Turbulence Characteristics in Skimming Flows on Stepped Spillways. Canadian Journal of Civil Engineering, Vol. 35, No. 9, pp. 865-880 (DOI:10.1139/L08-030) (2008)

Cartellier, A. Simultaneous Void Fraction Measurement, Bubble Velocity, and Size Estimate using a Single Optical Probe in Gas-Liquid Tow-Phase Flows. Rev. Sci. Instrum., Vol. 63, No. 11, pp. 5442-5453 (1992)

Cartellier, A., and Barrau, E. Monofiber Optical Probes for Gas Detection and Gas Velocity Measurements: Conical Probes. Intl Jl of Multiphase Flow, Vol. 24, No. 8, pp. 1265-1294 (1998)

Chanson, H. Hydraulics of Skimming Flows over Stepped Channels and Spillways. Journal of Hydraulic Research, IAHR, Vol. 32, No. 3, pp. 445-460 (1994)

Chanson, H. Air Bubble Entrainment in Free-Surface Turbulent Shear Flows. Academic Press, London, UK, 401 pages (1997)

Chanson, H. The Hydraulics of Stepped Chutes and Spillways. Balkema, Lisse, The Netherlands (2001)

Chanson, H. Air-Water Flow Measurements with Intrusive Phase-Detection Probes. Can we Improve their Interpretation? Journal of Hydraulic Engineering, ASCE, Vol. 128, No. 3, pp. 252-255 (2002)

Chanson, H. Turbulent Air-water Flows in Hydraulic Structures: Dynamic Similarity and Scale Effects. Environmental Fluid Mechanics, Vol. 9, No. 2, pp. 125-142 (DOI: 10.1007/s10652-008-9078-3) (2009)

Chanson, H., and Carosi, G. Turbulent Time and Length Scale Measurements in High-Velocity Open Channel Flows. Experiments in Fluids, Vol. 42, No. 3, pp. 385-401 (DOI 10.1007/s00348-006-0246-2) (2007)

Chanson, H., and Carosi, G. Advanced Post-Processing and Correlation Analyses in High-Velocity Air-Water Flows. Environmental Fluid Mechanics, Vol. 7, No. 6, pp. 495-508 (DOI 10.1007/s10652-007-9038-3) (1987b)

Chanson, H., and Toombes, L. Air-Water Flows down Stepped chutes: Turbulence and Flow Structure Observations. International Journal of Multiphase Flow, Vol. 27, No. 11, pp. 1737-1761 (2002)

Chanson, H., Yasuda, Y., and Ohtsu, I. Flow Resistance in Skimming Flows and its Modelling. Canadian Journal of Civil Engineering, Vol. 29, No. 6, pp. 809-819 (2002)

Coleman, S.E., Nikora, V.I., McLean, S.R., and Schlicke, E. Spatially-Averaged Turbulent Flow over Square Ribs. Jl of Engineering Mechanics, Vol. 133, No. 2, pp. 194-204 (2007)

Djenidi, L., Elavarasan, R., and Antonia, R.A. The Turbulent Boundary Layer over Transverse Square Cavities. Jl Fluid Mech., Vol. 395, pp. 271-294 (1999)

Felder, S., and Chanson, H. Turbulence, Dynamic Similarity and Scale Effects in High-Velocity Free-Surface Flows above a Stepped Chute. Experiments in Fluids, Vol. 47, No. 1, pp. 1-18 (DOI: 10.1007/s00348-009-0628-3) (2009)

Gonzalez, C.A., and Chanson, H. Interactions between Cavity Flow and Main Stream Skimming Flows: an Experimental Study. Canadian Journal of Civil Engineering, Vol. 31, No. 1, pp. 33-44 (2004)

Gonzalez, C.A., and Chanson, H. Experimental Measurements of Velocity and Pressure Distribution on a Large Broad-Crested Weir. Flow Measurement and Instrumentation, Vol. 18, No. 3-4, pp. 107-113 (DOI 10.1016/j.flowmeasinst.2007.05.005) (2007)

Gonzalez, C.A., and Chanson, H. Turbulence Manipulation in Embankment Stepped Chute Flows: an Experimental Study. European Journal of Mechanics B/Fluids, Vol. 27, No. 4, pp. 388-408 (DOI: 10.1016/j.euromechflu.2007.09.003) (2008)

Henderson, F.M. Open Channel Flow. MacMillan Company,

New York, USA (1966)

Herringe, R.A. A Study of the Structure of Gas-Liquid Mixture Flows. Ph.D. thesis, Univ. of New South Wales, Kensington, Australia (1973)

Herringe, R.A., and Davis, M.R. Detection of Instantaneous Phase Changes in Gas-Liquid Mixtures. Jl. of Physics E: Scientific Instruments, Vol. 7, pp. 807-812 (1974)

Jempson, M.A. Flood and Debris Loads on Bridges. Ph.D. thesis, Univ. of Queensland, Dept. of Civil Eng., Australia, May, 429 pages (2001)

Kobus, H. Scale Effects in Modelling Hydraulic Structures. Proc. Intl Symp. on Scale Effects in Modelling Hydraulic Structures, IAHR, Esslingen, Germany (1984)

Jones, O.C., and Delhaye, J.M. Transient and Statistical Measurement Techniques for two-Phase Flows : a Critical Review. Intl Jl of Multiphase Flow, Vol. 3, pp. 89-116 (1976)

Lin, J.C., and Rockwell, D. Organized Oscillations of Initially Turbulent Flow past a Cavity. AIAA Jl, Vol. 39, No. 6, pp. 1139-1151 (2001)

Matos, J. Hydraulic Design of Stepped Spillways over RCC Dams. Intl Workshop on Hydraulics of Stepped Spillways, Zürich, Switzerland, H.E. Minor & W.H. Hager Editors, Balkema Publ., pp. 187-194 (2000)

Neal, L.S., and Bankoff, S.G. A High Resolution Resistivity Probe for Determination of Local Void Properties in Gas-Liquid Flows. Am. Inst. Chem. Jl, Vol. 9, pp. 49-54 (1963)

Serizawa, A., Kataoka, I., and Michiyoshi, I. Turbulence Structure of Air-Water Bubbly Flows - I. Measuring Techniques. Intl Jl Multiphase Flow, Vol. 2, No. 3, pp. 221-233 (1975)

Tachie, M.F., and Adane, K.K. PIV Study of shallow Open Channel Flow over d- and k-type Transverse Ribs. Jl of Fluids Eng., ASME, Vol. 129, pp. 1058-1072

Toombes, L. Experimental Study of Air-Water Flow Properties on Low-Gradient Stepped Cascades. Ph.D. thesis, Dept of Civil Engineering, The University of Queensland (2002)

Toombes, L., and Chanson, H. Interfacial Aeration and Bubble Count Rate Distributions in a Supercritical Flow Past a Backward-Facing Step. International Journal of Multiphase Flow, Vol. 34, No. 5, pp. 427-436 (doi.org/10.1016/j.ijmultiphaseflow.2008.01.005) (2008)

Wood, I.R. Air Entrainment in Free-Surface Flows." IAHR Hydraulic Structures Design Manual No. 4, Hydraulic Design Considerations, Balkema Publ., Rotterdam, The Netherlands, 149 pages (1991)

Yasuda, Y., and Chanson, H. Micro- and Macro-scopic Study of Two-Phase Flow on a Stepped Chute. Proc. 30th IAHR Biennial Congress, Thessaloniki, Greece, J. Ganoulis and P. Prinos Ed., Vol. D, pp. 695-702 (2003)